

# Cellulose synthase complexes act in a concerted fashion to synthesize highly aggregated cellulose in secondary cell walls of plants

Shundai Li<sup>a,1</sup>, Logan Bashline<sup>a,1</sup>, Yunzhen Zheng<sup>b</sup>, Xiaoran Xin<sup>a</sup>, Shixin Huang<sup>c</sup>, Zhaosheng Kong<sup>d</sup>, Seong H. Kim<sup>c</sup>, Daniel J. Cosgrove<sup>b,2</sup>, and Ying Gu<sup>a,2</sup>

<sup>a</sup>Department of Biochemistry and Molecular Biology, Pennsylvania State University, University Park, PA 16802; <sup>b</sup>Department of Biology, Pennsylvania State University, University Park, PA 16802; <sup>c</sup>Chemical Engineering and Materials Research Institute, Pennsylvania State University, University Park, PA 16802; and <sup>d</sup>State Key Laboratory of Plant Genomics, Institute of Microbiology, Chinese Academy of Sciences, Beijing 100101, China

Contributed by Daniel J. Cosgrove, August 10, 2016 (sent for review July 5, 2016; reviewed by Ram Dixit and Simon R. Turner)

Cellulose, often touted as the most abundant biopolymer on Earth, is a critical component of the plant cell wall and is synthesized by plasma membrane-spanning cellulose synthase (CESA) enzymes, which in plants are organized into rosette-like CESA complexes (CSCs). Plants construct two types of cell walls, primary cell walls (PCWs) and secondary cell walls (SCWs), which differ in composition, structure, and purpose. Cellulose in PCWs and SCWs is chemically identical but has different physical characteristics. During PCW synthesis, multiple dispersed CSCs move along a shared linear track in opposing directions while synthesizing cellulose microfibrils with low aggregation. In contrast, during SCW synthesis, we observed swaths of densely arranged CSCs that moved in the same direction along tracks while synthesizing cellulose microfibrils that became highly aggregated. Our data support a model in which distinct spatiotemporal features of active CSCs during PCW and SCW synthesis contribute to the formation of cellulose with distinct structure and organization in PCWs and SCWs of *Arabidopsis thaliana*. This study provides a foundation for understanding differences in the formation, structure, and organization of cellulose in PCWs and SCWs.

cellulose synthase complex | live-cell imaging | cellulose microfibrils | plasma membrane | protein dynamics

Plant cell walls are predominantly composed of a complex matrix of polysaccharides, of which cellulose is the most abundant. Plant cells control the mechanical properties of the wall by organizing the synthesis and deposition of wall polymers and by modifying the wall architecture according to the needs of the cell. Primary cell walls (PCWs) have a multilamellate arrangement of cellulose microfibrils to accommodate growth while maintaining structural integrity (1). Certain cell types, such as fiber cells and vascular cells, subsequently form thick secondary cell walls (SCWs) with high cellulose content to structurally support the plant and to facilitate water transport (2). The composition of PCWs and SCWs differ. For instance, xyloglucan is the major hemicellulose of PCWs, whereas xylan is the major hemicellulose of SCWs in *Arabidopsis* (3, 4). Furthermore, the matrix polysaccharide, pectin, comprises a large proportion of PCWs, but only a small amount of pectin exists in SCWs (5), whereas the phenolic polymer, lignin, exclusively exists in SCWs and is not present in PCWs (2). Although both PCWs and SCWs contain cellulose, the organization and physical characteristics of cellulose in PCWs and SCWs differ (2), and yet little is known about how these differences arise. Genetic studies have revealed that different isoforms of cellulose synthase (CESA) proteins are responsible for cellulose synthesis during PCW and SCW synthesis. CESA1, -3, and -6-like (CESA6, -2, -5, and -9) proteins collaborate in the synthesis of PCW cellulose, whereas CESA4, -7, and -8 proteins are each necessary for SCW cellulose synthesis (6–8). In plants, CESAs are assembled into large, multimeric, rosette-shaped, plasma membrane (PM)-spanning CESA complexes (CSCs), each of which is thought to synthesize a single cellulose microfibril

(9–11). As cellulose is synthesized, CSCs glide laterally within the plane of the PM along linear trajectories that coincide with underlying cortical microtubules (CMTs), a phenomenon that can be observed by live-cell imaging of fluorescent protein-tagged CSCs (12). Live-cell imaging of CSCs has become influential not only in understanding CSC dynamics during cellulose synthesis, but also in understanding the trafficking of CSCs to and from the PM, dissecting the relationship between CSCs and CMTs, and characterizing the roles of CSC proteins and other proteins that influence cellulose synthesis (13–20). However, nearly all studies with live-cell imaging of CSCs to date have been conducted during PCW synthesis in epidermal cells. Until recently, similar image analyses during SCW synthesis have been thwarted due to limitations in imaging SCW-synthesizing cells, which are positioned deep within plant tissues (21). The inducible transdifferentiation of epidermal cells into SCW-synthesizing xylem-like cells now facilitates live-cell imaging of CSCs during SCW synthesis and allows for the comparison of CSC behavior during PCW and SCW synthesis (22). With this approach, we discovered distinct changes in the distribution and behavior of active CSCs during SCW synthesis, which contribute to the synthesis of cellulose microfibrils with distinct physical characteristics in SCWs.

## Significance

Plant cell walls are important in plant development and for textiles, wood products, and bioenergy. Cellulose, the microfibrillar component of primary cell walls (PCWs) and secondary cell walls (SCWs), is formed by cellulose synthase complexes (CSCs) at the plasma membrane. Here, we show that CSCs behave differently during PCW and SCW synthesis and form microfibrils with different organization. During PCW synthesis, dispersed CSCs synthesize cellulose microfibrils with low aggregation, whereas during SCW synthesis, densely arranged groups of CSCs move coherently to synthesize highly aggregated microfibrils. Our study suggests that controlled alterations in CSC distribution and orchestrated movements contribute to the high density and bundling of cellulose microfibrils in SCWs.

Author contributions: S.L., L.B., D.J.C., and Y.G. designed research; S.L., L.B., Y.Z., X.X., and S.H. performed research; S.L., Z.K., and D.J.C. contributed new reagents/analytic tools; S.L., L.B., Y.Z., X.X., S.H., S.H.K., D.J.C., and Y.G. analyzed data; and S.L., L.B., S.H., D.J.C., and Y.G. wrote the paper.

Reviewers: R.D., Washington University; and S.R.T., University of Manchester.

The authors declare no conflict of interest.

Freely available online through the PNAS open access option.

<sup>1</sup>S.L. and L.B. contributed equally to this work.

<sup>2</sup>To whom correspondence may be addressed. Email: dcosgrove@psu.edu or yug13@psu.edu.

This article contains supporting information online at [www.pnas.org/lookup/suppl/doi:10.1073/pnas.1613273113/-DCSupplemental](http://www.pnas.org/lookup/suppl/doi:10.1073/pnas.1613273113/-DCSupplemental).

## Results

**Transdifferentiated Cells Synthesize SCWs with Highly Aggregated Cellulose Microfibrils.** Similar to previous inducible xylem transdifferentiation systems (22, 23), we generated plants expressing the master regulator of xylem differentiation, Vascular-related NAC-domain 7, fused to the glucocorticoid receptor (35S::VND7-GR), and induced transdifferentiation by dexamethasone (DEX) treatment. Approximately 80% of epidermal cells of etiolated seedlings transdifferentiated after 60-h DEX treatment as indicated by lignin autofluorescence in SCW thickenings (Fig. 1*A*). SCW thickenings were also observed in epidermal peels from transdifferentiated seedlings using field emission scanning electron microscopy (FE-SEM) (Fig. 1*B*). Focused ion beam ablation was used to create windows through which the most recently deposited layer of cellulose microfibrils was observed (Fig. 1*C*). Cellulose microfibrils of SCWs in transdifferentiated cells were aggregated into bundles both within the lignified cell wall thickenings and in the nonlignified regions between thickenings (Fig. 1*D* and *G*). In contrast, cellulose microfibrils of PCWs from epidermal peels of nontransdifferentiated control seedlings were much less aggregated (Fig. 1*E* and *F*). Sum-frequency generation (SFG) vibrational spectroscopy, which can selectively detect the orientation and lateral packing of cellulose microfibrils in intact plant cell walls, showed that transdifferentiated seedlings exhibited spectral features similar to native SCWs in *Arabidopsis* stems (24), suggesting that the cell walls of transdifferentiated seedlings were structurally similar to native SCWs (Fig. 1*H*). The 2,944  $\text{cm}^{-1}$  and 2,868  $\text{cm}^{-1}$  alkyl stretch peaks of transdifferentiated seedlings indicate highly ordered cellulose, perhaps due to high cellulose aggregation, and the enhancement of 3,320  $\text{cm}^{-1}$  and 3,440  $\text{cm}^{-1}$  hydroxyl stretch peaks suggest that transdifferentiated seedlings have an elevated crystalline cellulose content (Fig. 1*H*) (24, 25). Analogous spectral features were absent in nontransdifferentiated seedlings where the PCW-related 2,904  $\text{cm}^{-1}$  peak was dominant (Fig. 1*H*) (24).

**Active CSCs Are Evenly Distributed Early in Transdifferentiation and Are Later Distributed Within Confined Hoops During the Synthesis of SCW Thickenings.** Having established a system in which epidermal cells reliably transdifferentiate into xylem-like cells with genuine SCWs, we investigated whether differences in the spatiotemporal behavior of CSCs during PCW and SCW synthesis could explain the structural differences of cellulose microfibrils in PCWs and SCWs. We generated a line expressing green fluorescent protein (GFP) fused to CESA7 driven by the native CESA7 promoter (ProCESA7::GFP-CESA7) that was able to rescue the growth phenotype of the null *cesa7<sup>mx3-1</sup>* mutant (Fig. S1*A*) and crossed it with 35S::VND7-GR. When 3-d-old etiolated seedlings were treated with DEX for 24 h, GFP-CESA7 was observed in cells undergoing transdifferentiation (Fig. S1*C* and *D*). Like CSC markers during PCW formation, such as GFP-CESA3, GFP-CESA7 labeled active CSCs at the PM and intracellular Golgi bodies (Fig. S1*B–D*) (12, 15, 16). In addition to localizing to distinct puncta, PM-localized GFP-CESA7 localized to swaths of motile signal, which might represent stretches of densely arranged CSCs (Fig. 2*D*, *F*, *G*, *I*, *J*, and *L*, Fig. S1*C* and *D*, and Movie S1). Early in transdifferentiation PM-localized GFP-CESA7 particles were positioned along tracks that were distributed evenly across the cell surface (Fig. 2*D* and Fig. S1*C*). Later, GFP-CESA7 became focused within defined hoop-like regions of the PM (Fig. 2*G* and Fig. S1*D*), which is consistent with previous observations (22). These observations suggest that a uniform layer of SCW is synthesized over the entire cell surface before hoop formation, which is probably the source of highly aggregated cellulose in the non-lignified regions between cell wall thickenings (Fig. 1*D*), and that SCW thickenings are subsequently formed when CSC distribution is constrained within hoop regions.

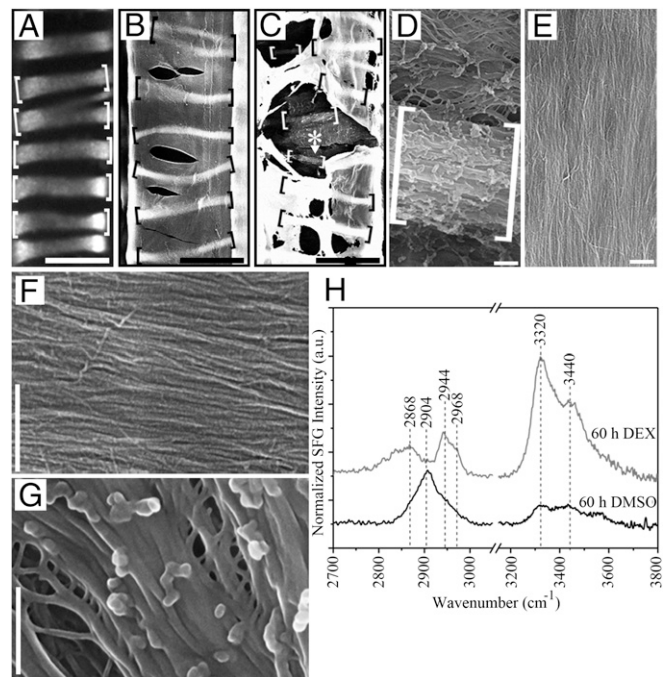


**Fig. 1.** SCWs of transdifferentiated xylem cells exhibit highly aggregated, bundled cellulose microfibrils and exhibit spectral characteristics that are similar to native SCWs. (A–G) 35S::VND7-GR seedlings were treated for 60 h with 20  $\mu\text{M}$  DEX to induce transdifferentiation (A–D and G) or an equal volume of the solvent, dimethyl sulfoxide (DMSO), as a nontransdifferentiation control (E and F). White brackets denote autofluorescent lignified SCW thickenings in a confocal image (A). Black brackets denote SCW thickenings in FE-SEM images of intact transdifferentiated cells of an epidermal peel (B and C). White brackets denote SCW thickenings at the inner surface of transdifferentiated cells that were broken open with a focused ion beam (C and D). The asterisk arrowhead in C indicates the region magnified in D. Cellulose microfibrils of PCWs at the inner surface of DMSO control, nontransdifferentiated epidermal cells are less bundled (E and F) than those of SCWs in transdifferentiated cells (D and G). (Scale bars: A–C, 10  $\mu\text{m}$ ; D–G, 200 nm.) (H) Representative SFG spectra from DMSO control, nontransdifferentiated (black) and DEX-treated, transdifferentiated (gray) seedlings.

**Active CSCs Exhibit Bidirectional Movement During PCW Synthesis and Directionally Coherent Movement During SCW Synthesis.** The striking changes in CSC distribution during transdifferentiation caused us to investigate whether CSCs also developed unique dynamic features. Both during PCW and SCW synthesis, PM-localized CSCs moved steadily along linear trajectories (Fig. 2*A*, *D*, and *G* and Movie S1), which occurs during active cellulose synthesis (11, 12). The velocities of several CSC markers have been recorded during PCW synthesis (6, 7, 12, 13, 16, 17, 19, 22, 26, 27), each exhibiting a slight variation in velocity, which makes the direct comparison of the velocities of two dissimilar CSC markers difficult. To account for the marker-to-marker variation in CSC velocity, the velocities of several CSC markers were measured during PCW synthesis and compared with the velocities of GFP-CESA7-labeled CSCs during SCW synthesis (Fig. S2). The velocities of GFP-CESA7-labeled CSCs during SCW synthesis in this study were similar to recent measurements of YFP-CESA7 particles during SCW synthesis (22). However, these velocities of CSCs during SCW synthesis fall within the range of velocities exhibited by CSC markers during PCW synthesis, making it uncertain whether CSC velocities are meaningfully different during PCW and SCW synthesis (Fig. S2).

However, other aspects of CSC dynamics were significantly different during PCW and SCW synthesis. In contrast to the bidirectional movement of CSCs along shared tracks during PCW synthesis (12), a majority of CSCs moved coherently in a favored direction along shared tracks during SCW synthesis. The

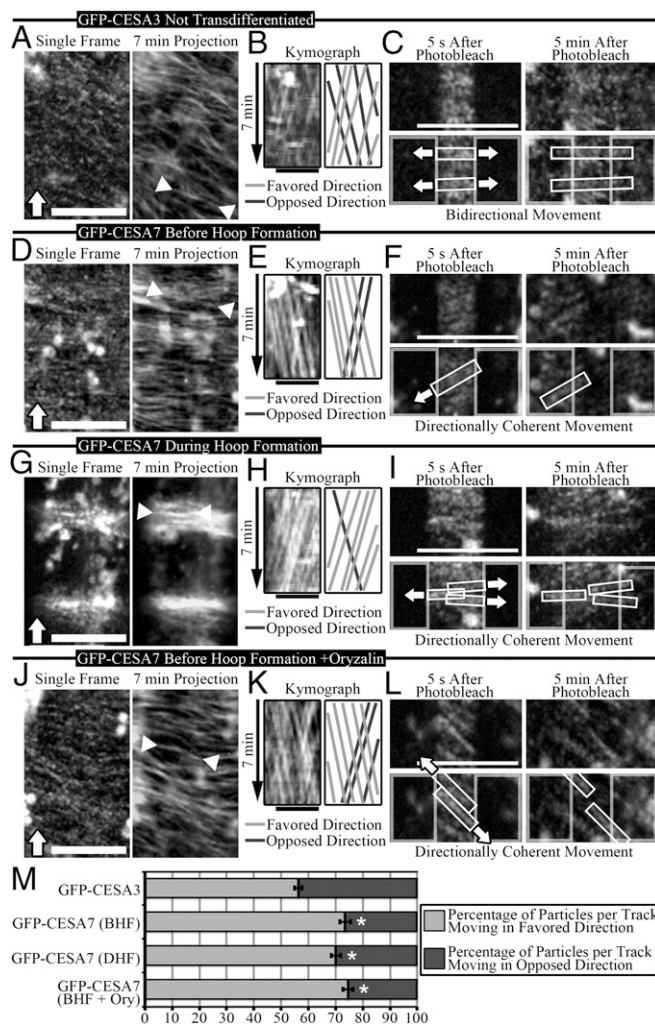


**Fig. 2.** Active CSCs exhibit bidirectional movement along tracks during PCW synthesis and directionally coherent movement along tracks during SCW synthesis. (A–L) GFP-CESA3 *cesa3<sup>le5</sup>* was imaged in nontransdifferentiating cells as a CSC marker during PCW synthesis (A–C), and GFP-CESA7 *cesa7<sup>px3-1</sup> 35S::VND7-GR* was imaged during two stages of xylem cell transdifferentiation, before hoop formation (BHF) and during hoop formation (DHF), as a CSC marker during SCW synthesis (D–L). (J–L) The influence of CMTs on GFP-CESA7 particle behavior was assessed via 8–12 h treatment with 25  $\mu$ M oryzalin. (A, D, G, and J) Representative single-frame images and 7-min projection images show the distribution and trajectories of GFP-CESA particles, respectively. Arrows indicate the apical direction. (Scale bars: 10  $\mu$ m.) (B, E, H, and K) Kymographs were derived from the indicated tracks in each 7-min projection image and the directions of particle movements along the track were color-coded in schematic kymographs. (Scale bars: 5  $\mu$ m.) (C, F, I, and L) Images from 5 s and 5 min after photobleaching the lateral sides of cells are shown to depict the direction of particle movement along tracks of interest. Upper images are raw images, and lower images are highlighted to show the bleached regions (gray boxes), the particles within tracks of interest (white boxes), and the favored direction of particle movements (arrows). (Scale bars: 10  $\mu$ m.) The frequency of particle direction along individual tracks was quantified (M). Error bars are standard errors of the mean;  $n \geq 48$  tracks and 6 seedlings per data point. \* $P < 0.0001$ .

crosshatched pattern of trajectories in kymographs from GFP-CESA3-labeled CSCs during PCW synthesis is indicative of bidirectional CSC movement (Fig. 2B and M), whereas trajectories on kymographs from GFP-CESA7-labeled CSCs mostly run in a common direction during SCW synthesis both before and during hoop formation (Fig. 2E, H, and M). The directionally coherent movement of GFP-CESA7 existed on a track-by-track

basis such that distinct tracks could exhibit coherent particle movement in opposite directions, resulting in no net directional bias on a cell-wide scale and an antiparallel packing of cellulose microfibrils in SCWs at the mesoscale (25). Adjacent CSC tracks became condensed within the hoop regions, which sometimes obscured the ability to resolve individual tracks and potentially caused an underrepresentation of directional coherence in the quantification during hoop formation (Fig. 2M). Likewise, in a recent study, a kymograph of motile YFP-CESA7 particles displayed a cross-hatched pattern, which would seem to suggest that CSCs moved bidirectionally during SCW synthesis (22). However, it is likely that the kymograph in the previous study encompassed particles from multiple adjacent tracks due to the close packing of adjacent tracks during hoop formation and due to technical differences in the kymograph generation methods of the two studies (ref. 22 and *Materials and Methods*).

To more clearly visualize the directional trends of CSC movement, a lateral photobleaching experiment was designed in which the lateral regions of the cell were bleached during time-lapse imaging and the direction of the movement of the remaining unbleached particles within a central strip of the cell was monitored after photobleaching (Fig. 2C, F, and I and *Movie S2*). To better analyze the direction of the movement of the CSC from unbleached region to bleached region without influence of newly delivered CSCs, we selected photobleaching regions with minimal underlying CESA-associated intracellular compartments. The bidirectional movement of GFP-CESA3 during PCW synthesis resulted in an equal number of particles on each track moving into the left and right bleached regions (Fig. 2C). The directionally coherent movement of GFP-CESA7 during SCW synthesis resulted in an uneven distribution of signal from each track moving into the left and right bleached regions before and during hoop formation (Fig. 2F and I). In many cases, swaths of GFP-CESA7 signal, rather than distinct particles, moved coherently during SCW synthesis, which might represent groups of CSCs that are too crowded to be resolved as individual particles by light microscopy.

**Cortical Microtubules Are Not Required to Maintain the Directionally Coherent Movement of Active CSCs During SCW Synthesis.** We next asked whether the directional coherence of CSC movement was controlled by the CMTs along which the CSCs travel (12, 22). Because End Binding Protein 1B (EB1b) follows the plus-ends of polymerizing microtubules, Red Fluorescent Protein (RFP)-conjugated EB1b (RFP-EB1b) can be used as a marker for the position and polarity of newly formed microtubules. Like GFP-CESA7 particles, RFP-EB1b particles were distributed evenly across the cell early in transdifferentiation and became restricted to hoop-like regions at later stages of transdifferentiation during the synthesis of SCW thickenings. The trajectories of GFP-CESA7 and RFP-EB1b were often colocalized (Fig. S3A). Kymographs were created from colocalized GFP-CESA7 and RFP-EB1b trajectories, and the direction of coherent CSC movement was compared with the CMT polarity of each track. The direction of coherent CSC movement had a similar tendency to travel toward the plus-end of CMT tracks and toward the minus-end of CMT tracks (Fig. S3B–G), suggesting that there is no correlation between the polarities of newly formed CMTs and the direction of coherent CSC movement.

Pharmacological disruption of CMTs was used to further probe the role of CMTs during SCW synthesis. After 8–12 h of treatment with 25  $\mu$ M oryzalin, a microtubule-depolymerizing drug, RFP-EB1b particles were abolished in transdifferentiating cells, indicating that the polymerization of new CMTs was arrested (Fig. S4A and B). Under the same oryzalin treatment conditions, the microtubule marker, GFP-Microtubule Associated Protein4 (GFP-MAP4), no longer localized to CMTs, but rather in the cytosol, suggesting that CMT arrays were abolished (Fig. S4C and D). In transdifferentiating cells, oryzalin treatment occasionally caused GFP-CESA7 trajectories to appear wavy but did not influence the

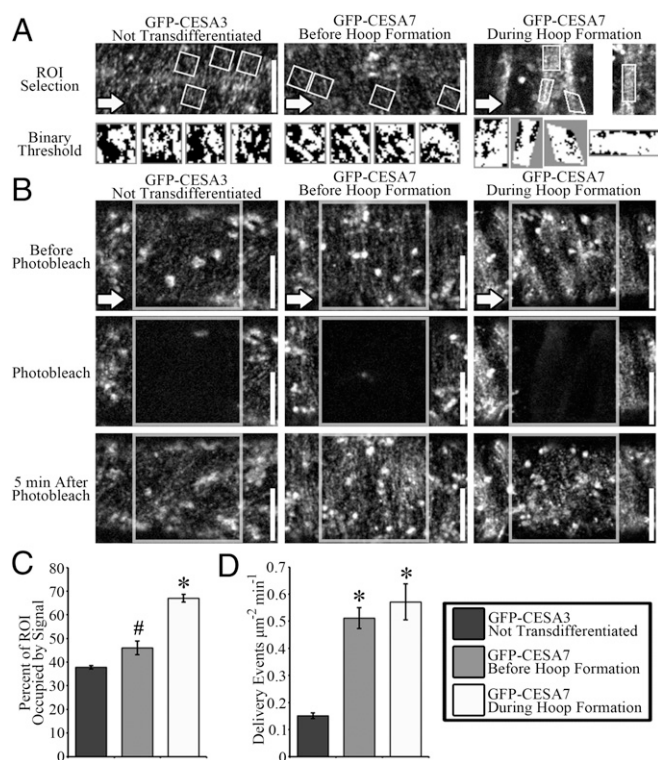


**Fig. 3.** CSCs are densely distributed within hoop regions during SCW synthesis, and CSC delivery to the PM occurs at an elevated rate during SCW synthesis compared with PCW synthesis. (A) ROIs (white shapes) that exclusively contain signal from PM-localized CSCs display areas occupied by signal in white from images of GFP-CESA3 during PCW synthesis (Left) and GFP-CESA7 during SCW synthesis both before (Center) and during (Right) hoop formation. (B) The delivery of CSCs to the PM was visualized by photobleaching a ROI (gray box) and recording the repopulation of PM CSCs within the bleached region. Time points preceding the bleach (Upper), immediately following the bleach (Middle), and 5 min after the bleach (Lower) are shown. Arrows denote the apical direction (A and B). (Scale bars: 10  $\mu\text{m}$ .) (C) The percentage of area of ROIs occupied by signal was quantified. Error bars are SEM;  $n \geq 28$  ROIs from  $\geq 7$  cells per data point.  $^{\#}P = 0.028$ ;  $^*P < 0.0001$ . (D) The rate of delivery of CSCs to the PM was quantified from photobleaching experiments. Error bars are standard errors of the mean;  $n \geq 7$  cells per data point.  $^*P < 0.0001$ .

directional coherence or velocity of GFP-CESA7 movement (Fig. 2J–M and Fig. S2). These data suggest that CMTs influence CSC trajectories but do not play a role in maintaining the directional coherence of CSC movement during SCW formation.

**An Elevated Rate of CSC Delivery to the Plasma Membrane During SCW Synthesis Results in the Crowding of CSCs During SCW Synthesis.** Because CMTs do not participate in the maintenance of directionally coherent CSC movement, the directionally coherent movement might be indicative of populations of CSCs working in a concerted fashion during SCW synthesis, perhaps through passive crowding of CSCs in the PM or through the establishment of physical contacts between neighboring CSCs. Early freeze–fracture electron microscopy studies showed high densities—up to 135 or 191 CSCs per square micron—and clustering of CSCs at the sites of developing cell wall thickenings in xylem cells of various higher plants (28–30). Although light microscopy is incapable of resolving such high densities of particles, the coherently moving swaths of GFP-CESA7 signal described previously might be symptomatic of CSC crowding (Fig. 2 and Movie S2). As a rough assessment of PM-localized CSC populations during PCW and SCW synthesis, we measured the percentage of PM area occupied by GFP-CESA3 or GFP-CESA7 within regions of interest (ROIs) that were devoid

of underlying intracellular signal (Fig. 3A). During SCW synthesis, GFP-CESA7 occupied a slightly higher percentage of the PM area before hoop formation than GFP-CESA3 during PCW synthesis (Fig. 3A and C). During hoop formation, a high percentage of the PM was occupied by GFP-CESA7 signal within hoop regions, but the area between hoops was nearly devoid of PM-localized signal (Fig. 3A and C). Under the presumption that the maintenance of crowded populations of CSCs during SCW synthesis would require high rates of CSC delivery to the PM, the delivery rate of CSCs to the PM was measured via photobleaching experiments and compared during PCW and SCW synthesis (Fig. 3B and Movie S3). Both before and during hoop formation, GFP-CESA7-labeled particles were delivered to the PM at more than triple the rate of GFP-CESA3 particles during PCW synthesis (Fig. 3B and D). During hoop formation, delivery of new PM-localized GFP-CESA7 particles was confined to the hoop regions. The elevated rates of CSC delivery during SCW synthesis and the more extensive coverage of PM area that we observed, along with previous electron microscopy measurements of high CSC density under developing SCW thickenings, suggest that CSCs are arranged in crowded groups during SCW synthesis (29–32).

## Discussion

Cellulose is synthesized by diverse organisms, including plants, algae, tunicates, protists, fungi, and bacteria (28, 31). CESAs of these divergent organisms are organized in a variety of spatial arrangements—including rows of CESAs, linear arrays of CESAs, and rosette-shaped complexes of CESAs—which dictate the size, shape, and aggregation of the cellulose that is produced by each organism (33, 34). It has also been shown that some organisms can alter the spatial arrangement of CESAs to alter the structure of the cellulose being produced. For example, freeze–fracture electron microscopy studies of the green algae, *Microsterias denticulata*, showed that *Microsterias* uses a sparse population of disperse rosette CSCs to synthesize randomly oriented arrays of cellulose during PCW synthesis and uses large, clustered arrays of rosette CSCs to synthesize highly aggregated bands of cellulose during SCW synthesis (35). Freeze–fracture electron microscopy has also shown that individual rosette CSCs are capable of synthesizing cellulose in higher plants, but some investigators have speculated that clusters and groups of rosette CSCs that are positioned along shared cellulose microfibril impressions might cooperate to synthesize bundled cellulose microfibrils in SCWs (29, 30, 32). Now—with dynamic, spatiotemporal details of CSC behavior during PCW and SCW synthesis in living plants—we can propose a hypothetical model to explain how plants synthesize PCWs with low cellulose microfibril aggregation and SCWs with highly aggregated and bundled cellulose microfibrils by altering the behavior of active CSCs at the PM (Fig. 4).

Our data are consistent with the following hypothetical model. Cellulose of low aggregation is synthesized by disperse CSCs that exhibit bidirectional movement during PCW synthesis (Fig. 4A and B). During SCW synthesis, elevated rates of CSC delivery to the PM produce crowded populations of closely arranged CSCs, which move in a coherent direction during cellulose synthesis. The concerted activity of coherently moving and densely arranged CSCs during SCW synthesis results in the synchronous extrusion of many closely spaced cellulose microfibrils, promoting the aggregation and bundling of adjacent microfibrils at the time of synthesis (Fig. 4C–E).

As of yet, it is unclear whether the coherent movement of CSCs occurs passively or through an unknown regulated process. In either case, the observations that the coherent CSC movement occurs on a track-by-track basis and often involves swaths of CSC signal suggest that coherent CSC movement is a spatially confined process, potentially caused by the crowding or physical association of groups of CSCs at the PM (31, 32). Although the role of CMTs in the maintenance of the coherent movement of CSCs has been ruled out, the role of CMTs in the initial

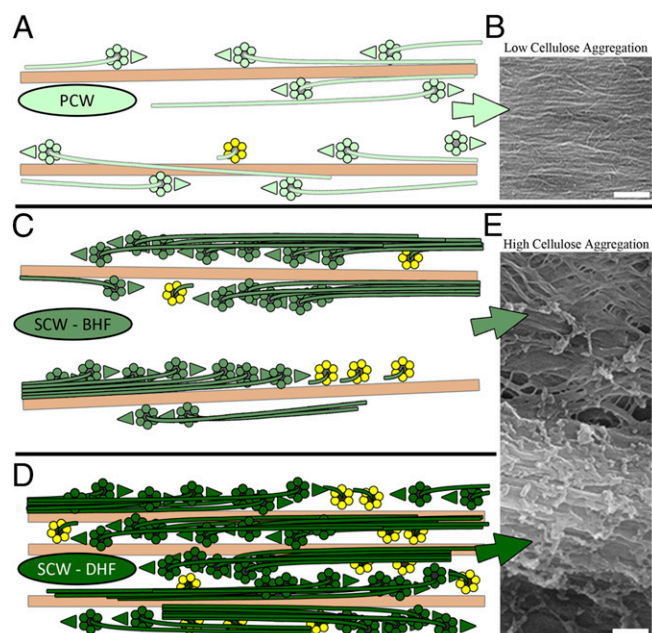


**Fig. 4.** The concerted activity of densely arranged and coherently moving CSCs is responsible for the synthesis of highly aggregated cellulose microfibrils during SCW production in transdifferentiating xylem cells. The model displays a schematic aerial view of cellulose synthesis during PCW synthesis (A and B) and during SCW synthesis before hoop formation (SCW - BHF) (C and E) and during hoop formation (SCW - DHF) (D and E) in transdifferentiating xylem cells. Green CSCs represent active CSCs, which travel along brown CMTs. Yellow CSCs represent newly delivered CSCs to emphasize the differences in delivery rate of CSCs during PCW and SCW synthesis. During PCW synthesis, relatively low rates of CSC delivery maintain a disperse distribution of CSC particles at the PM that exhibit bidirectional movement along CMTs during cellulose synthesis (A). The uncoordinated activity of primary CSCs produces cellulose microfibrils with low aggregation in PCWs (B). During SCW synthesis in transdifferentiating xylem cells, high rates of CSC delivery cause the crowding of swaths of active CSCs at the PM that move coherently in a common direction both before (C) and during (D) hoop formation. The concerted activity of groups of coherently moving CSCs causes the formation of the highly aggregated cellulose microfibrils of SCWs (E). During hoop formation, CMTs and CSCs become condensed and restricted to confined regions of the PM (D) to accommodate the synthesis of cellulose within SCW thickenings (E). (Scale bars: 200 nm.)

establishment of the coherent movement of CSCs and in other aspects of SCW synthesis remains to be tested.

In addition to the observed differences in CSC distribution and behavior during PCW and SCW synthesis, other differences between PCWs and SCWs might also contribute to the differences in cellulose microfibril aggregation. For example, it is unclear what role, if any, other components of the cell wall play in the aggregation status of cellulose microfibrils in PCWs and SCWs. Several models for the interaction of hemicelluloses—xyloglucan in PCWs and xylan in SCWs—with cellulose have been described (36, 37), suggesting that hemicellulose–cellulose interactions might influence cellulose aggregation. Another possibility could be that lignin contributes to the high aggregation of cellulose in SCWs. Immunofluorescence experiments showed that LM10-labeled xylan was localized to discrete regions of the cell wall defined by SCW thickenings in transdifferentiated xylem-like cells of *Arabidopsis* (38). Similarly, lignin and the laccase enzymes that catalyze lignin polymerization were confined to SCW thickenings in transdifferentiated xylem-like cells (Fig. 14) (38). Similar confinement of xylan/lignin within hoop regions may support their role in assisting cellulose aggregation during SCW synthesis. Interestingly, we observed highly aggregated cellulose microfibrils not only

within the SCW thickenings of transdifferentiated xylem-like cells but also in the nonlignified regions spanning between SCW thickenings that lack detectable LM10-labeled xylan (Fig. 1D) (38), suggesting that increased levels of cellulose aggregation might be possible without substantial contributions from xylan or lignin. Nevertheless, future studies should more thoroughly address the contribution of xylan and/or lignin in cellulose aggregation of SCWs, perhaps by combining the tools used in the current study with xylan- or lignin-deficient mutants. It is our hope that this study can serve as a foundation to help stimulate future investigations into how plants control and alter cell wall structure and synthesis.

## Materials and Methods

**Plasmid Construction.** proCESA7::GFP-CESA7, 35S::VND7-GR, and proEB1b::mCherry-EB1b were constructed by gateway cloning. See *SI Materials and Methods* for details on the construction.

**Plant Transformation and Generation of Lines.** CESA7 transfer DNA (SALK\_029940c, *irx3-4*) was obtained from the *Arabidopsis* Biological Resource Center and confirmed with the following primers: left genomic primer, 5'-AGAGAAGC-TTAAGGAACCGC-3'; right genomic primer, 5'-GAACAACACAGAGCAGAGGG-3'; and left T-DNA border primer, 5'-ATTTGCGGATTCGGAAC-3'. To obtain the GFP-CESA7 transgenic line, proCESA7::GFP-CESA7 was transformed into *irx3-4* using the floral dip method of Agrobacterium-mediated transformation. Both 35S::VND7-GR and proEB1b::mCherry-EB1b were transformed into WT (Col-0) *Arabidopsis*. A cross was made to obtain a line expressing both GFP-CESA7 and VND7-GR. To obtain a line expressing GFP-CESA7, VND7-GR, and mCherry-EB1b, a cross was made between a homozygous GFP-CESA7 line and a homozygous line containing VND7-GR and mCherry-EB1b.

Transgenic lines with markers of CSCs during PCW synthesis were previously described as follows: GFP-CESA3 *cesa3<sup>ies</sup>* (6), GFP-CESA3 *cesa3<sup>ies</sup>* RFP-TUA5 (16), mCherry-CESA3 *cesa3<sup>ies</sup>* (19), GFP-CESA5 (26), GFP-CESA6 *cesa6<sup>prc1-1</sup>* (6), YFP-CESA6 *cesa6<sup>prc1-1</sup>* RFP-TUA5 (16), mCherry-CESA6 *cesa6<sup>prc1-1</sup>* (13), GFP-CSI1 *csi1-3* (17), GFP-CSI3 *csi3-1* (17), RFP-CSI1 *csi1-6* (27), and GFP-KOR1 *kor1-3* (19).

**Induction of Transdifferentiation and Drug Treatment.** Seeds were surface sterilized with 30% (wt/vol) bleach for 15 min, washed three times with autoclaved double-distilled H<sub>2</sub>O (ddH<sub>2</sub>O), and stored at 4 °C for 3–7 d. Seeds were grown for 3 d at 21 °C in the dark on vertical half-strength Murashige and Skoog (MS) plates containing 1% sucrose. Three-day-old seedlings were placed in open microfuge tubes containing half-strength MS 3% (wt/vol) sucrose liquid medium that was supplemented with either 20 μM DEX for induced samples or an equivalent volume of the solvent, dimethyl sulfoxide (DMSO), for control seedlings. Seedlings that were subjected to live-cell fluorescence imaging were observed after 24–30 h of DEX treatment. In experiments in which microtubules were pharmacologically removed, oryzalin (25 μM) was introduced to the liquid induction medium after 16 h of induction and seedlings were imaged 8–12 h later. Seedlings that were subjected to SFG, FE-SEM, or lignin autofluorescence imaging were treated for 60 h with DEX or DMSO. After DEX or DMSO treatment, samples for SFG analysis were frozen on MS plates containing 1% sucrose at –80 °C overnight. After thawing, groups of 20–30 seedlings were aligned parallel to close to one another in a single layer on glass slides and air dried before SFG analysis. All other analyses were conducted on fresh, never-frozen, never-dried samples.

**SFG Vibrational Spectroscopy Analysis.** The broadband SFG spectroscopy system and common SFG spectra collecting procedures were previously described (19, 39). SFG spectroscopic probing was performed in the reflection geometry and s-polarized sum frequency output, s-polarized visible input, and p-polarized IR input (SFG, 800 nm, and IR, respectively) polarization combination. To account for inherent heterogeneity within each sample, SFG data collection was performed at four different locations on each sample and averaged to generate a representative SFG spectrum for each sample.

**FE-SEM.** Epidermal peels from DEX or DMSO-treated hypocotyls were gently shaken in buffer containing 20 mM Hepes and 0.1% Tween-20 for 2 h to remove membrane material and subjected to five 3-min washes with ddH<sub>2</sub>O. Peels were transferred to 200-mesh grids with the inner part of the peel facing up and treated with 100% (wt/vol) ethanol (USP KOPTec) for 30 min. Samples were dried with a Leica EM CPD300 automated critical point drier and coated with iridium using a Emitech K575X sputter coater. Images were obtained using a Zeiss Sigma VP-FESEM.

Cells of epidermal peels of transdifferentiated seedlings remained intact and required focused ion beam ablation to open the cells with an FEI Quanta 3D 200 focused ion beam. After focused ion beam ablation, samples were sputter-coated once again to coat the newly exposed regions and imaged.

**Live-Cell Imaging and Analysis.** The imaging system consisted of a Leica DMI6000 microscope with a Leica 100 $\times$ 1.4 NA oil objective, a Yokogawa CSUX1 spinning disk system, and a Photometrics QuantEM:512SC CCD camera as described previously (20). Acousto-optic tunable filter-controlled excitation lasers (491 nm for GFP and 561 nm for RFP and lignin autofluorescence) and emission filters

(520/50 nm for GFP and 620/60 nm for RFP and lignin autofluorescence) were used for fluorescence imaging. An integrated iLas photobleaching assembly (Roper Scientific) with a 405-nm laser was used for photobleaching experiments. Image acquisition was controlled using Metamorph (Molecular Devices) software. See *SI Materials and Methods* for details on image acquisition and data analysis.

**ACKNOWLEDGMENTS.** This work was supported by the Center for Ligno-Cellulose Structure and Formation, an Energy Frontier Research Center funded by the US Department of Energy, Office of Science, Basic Energy Sciences, under Award DE-SC0001090.

- Cosgrove DJ (2005) Growth of the plant cell wall. *Nat Rev Mol Cell Biol* 6(11):850–861.
- Cosgrove DJ, Jarvis MC (2012) Comparative structure and biomechanics of plant primary and secondary cell walls. *Front Plant Sci* 3:204.
- Kumar M, Campbell L, Turner S (2016) Secondary cell walls: Biosynthesis and manipulation. *J Exp Bot* 67(2):515–531.
- Pauly M, Keegstra K (2016) Biosynthesis of the plant cell wall matrix polysaccharide xyloglucan. *Annu Rev Plant Biol* 67:235–259.
- Anderson CT (2016) We be jammin': An update on pectin biosynthesis, trafficking and dynamics. *J Exp Bot* 67(2):495–502.
- Desprez T, et al. (2007) Organization of cellulose synthase complexes involved in primary cell wall synthesis in *Arabidopsis thaliana*. *Proc Natl Acad Sci USA* 104(39):15572–15577.
- Persson S, et al. (2007) Genetic evidence for three unique components in primary cell-wall cellulose synthase complexes in *Arabidopsis*. *Proc Natl Acad Sci USA* 104(39):15566–15571.
- Taylor NG, Howells RM, Huttly AK, Vickers K, Turner SR (2003) Interactions among three distinct CesA proteins essential for cellulose synthesis. *Proc Natl Acad Sci USA* 100(3):1450–1455.
- Hill JL, Jr, Hammudi MB, Tien M (2014) The *Arabidopsis* cellulose synthase complex: A proposed hexamer of CESA trimers in an equimolar stoichiometry. *Plant Cell* 26(12):4834–4842.
- Kimura S, et al. (1999) Immunogold labeling of rosette terminal cellulose-synthesizing complexes in the vascular plant *Vigna angularis*. *Plant Cell* 11(11):2075–2086.
- Somerville C (2006) Cellulose synthesis in higher plants. *Annu Rev Cell Dev Biol* 22:53–78.
- Paredez AR, Somerville CR, Ehrhardt DW (2006) Visualization of cellulose synthase demonstrates functional association with microtubules. *Science* 312(5779):1491–1495.
- Bashline L, Li S, Anderson CT, Lei L, Gu Y (2013) The endocytosis of cellulose synthase in *Arabidopsis* is dependent on  $\mu$ 2, a clathrin-mediated endocytosis adaptin. *Plant Physiol* 163(1):150–160.
- Bashline L, Li S, Zhu X, Gu Y (2015) The TWD40-2 protein and the AP2 complex cooperate in the clathrin-mediated endocytosis of cellulose synthase to regulate cellulose biosynthesis. *Proc Natl Acad Sci USA* 112(41):12870–12875.
- Crowell EF, et al. (2009) Pausing of Golgi bodies on microtubules regulates secretion of cellulose synthase complexes in *Arabidopsis*. *Plant Cell* 21(4):1141–1154.
- Gutierrez R, Lindeboom JJ, Paredez AR, Emons AM, Ehrhardt DW (2009) *Arabidopsis* cortical microtubules position cellulose synthase delivery to the plasma membrane and interact with cellulose synthase trafficking compartments. *Nat Cell Biol* 11(7):797–806.
- Lei L, Li S, Du J, Bashline L, Gu Y (2013) Cellulose synthase INTERACTIVE3 regulates cellulose biosynthesis in both a microtubule-dependent and microtubule-independent manner in *Arabidopsis*. *Plant Cell* 25(12):4912–4923.
- Lei L, et al. (2015) CELLULOSE SYNTHASE INTERACTIVE1 is required for fast recycling of cellulose synthase complexes to the plasma membrane in *Arabidopsis*. *Plant Cell* 27(10):2926–2940.
- Lei L, et al. (2014) The *jiaoyao1* mutant is an allele of *korrigan1* that abolishes endoglucanase activity and affects the organization of both cellulose microfibrils and microtubules in *Arabidopsis*. *Plant Cell* 26(6):2601–2616.
- Li S, Lei L, Somerville CR, Gu Y (2012) Cellulose synthase interactive protein 1 (CS11) links microtubules and cellulose synthase complexes. *Proc Natl Acad Sci USA* 109(1):185–190.
- Wightman R, Marshall R, Turner SR (2009) A cellulose synthase-containing compartment moves rapidly beneath sites of secondary wall synthesis. *Plant Cell Physiol* 50(3):584–594.
- Watanabe Y, et al. (2015) Visualization of cellulose synthases in *Arabidopsis* secondary cell walls. *Science* 350(6257):198–203.
- Yamaguchi M, et al. (2010) VASCULAR-RELATED NAC-DOMAIN6 and VASCULAR-RELATED NAC-DOMAIN7 effectively induce transdifferentiation into xylem vessel elements under control of an induction system. *Plant Physiol* 153(3):906–914.
- Park YB, et al. (2013) Monitoring meso-scale ordering of cellulose in intact plant cell walls using sum frequency generation spectroscopy. *Plant Physiol* 163(2):907–913.
- Lee CM, Kafle K, Park YB, Kim SH (2014) Probing crystal structure and mesoscale assembly of cellulose microfibrils in plant cell walls, tunicate tests, and bacterial films using vibrational sum frequency generation (SFG) spectroscopy. *Phys Chem Chem Phys* 16(22):10844–10853.
- Bischoff V, et al. (2011) Phytochrome regulation of cellulose synthesis in *Arabidopsis*. *Curr Biol* 21(21):1822–1827.
- Gu Y, et al. (2010) Identification of a cellulose synthase-associated protein required for cellulose biosynthesis. *Proc Natl Acad Sci USA* 107(29):12866–12871.
- Brown RM, Jr (1985) Cellulose microfibril assembly and orientation: Recent developments. *J Cell Sci Suppl* 2:13–32.
- Herth W (1985) Plasma-membrane rosettes involved in localized wall thickening during xylem vessel formation of *Lepidium sativum* L. *Planta* 164(1):12–21.
- Schneider B, Herth W (1986) Distribution of plasma-membrane rosettes and kinetics of cellulose formation in xylem development of higher-plants. *Protoplasma* 131(2):142–152.
- Baskin TI (2001) On the alignment of cellulose microfibrils by cortical microtubules: A review and a model. *Protoplasma* 215(1-4):150–171.
- Herth W (1984) Oriented rosette alignment during cellulose formation in mung bean hypocotyl. *Naturwissenschaften* 71(4):216–217.
- Itoh T, Kimura S, Brown RM, Jr (2007) Immunogold labeling of cellulose-synthesizing terminal complexes. *Cellulose: Molecular and Structural Biology*, eds Brown RM, Jr, Saxena IM (Springer, Dordrecht, The Netherlands), pp 237–256.
- Okuda K, Sekida S (2007) Cellulose-synthesizing complexes of a dinoflagellate and other unique algae. *Cellulose: Molecular and Structural Biology*, eds Brown RM, Jr, Saxena IM (Springer, Dordrecht, The Netherlands), pp 199–216.
- Giddings TH, Jr, Brower DL, Staehelin LA (1980) Visualization of particle complexes in the plasma membrane of *Micrasterias denticulata* associated with the formation of cellulose fibrils in primary and secondary cell walls. *J Cell Biol* 84(2):327–339.
- Busse-Wicher M, et al. (2016) Evolution of xylan substitution patterns in gymnosperms and angiosperms: Implications for xylan interaction with cellulose. *Plant Physiol* 171(4):2418–2431.
- Park YB, Cosgrove DJ (2012) A revised architecture of primary cell walls based on biomechanical changes induced by substrate-specific endoglucanases. *Plant Physiol* 158(4):1933–1943.
- Schuetz M, et al. (2014) Laccases direct lignification in the discrete secondary cell wall domains of protoxylem. *Plant Physiol* 166(2):798–807.
- Lee CM, Kafle K, Huang S, Kim SH (2016) Multimodal broadband vibrational sum frequency generation (MM-BB-V-SFG) spectrometer and microscope. *J Phys Chem B* 120(1):102–116.

# Supporting Information

Li et al. 10.1073/pnas.1613273113

## SI Materials and Methods

**Plasmid Construction.** To construct the *proCESA7::GFP-CESA7* construct, the promoter of *CESA7* (*At5G17420*) was amplified with primers 5'-CCCGGGGGTGGCAAGCTAGGATCGGA-3' and 5'-TCTAGAAGGGACGGCCGAGATTAGC-3' and cloned into *pCR8/GW/TOPO* (catalog no. K2500-20; Invitrogen) and sequenced. A *Sma*/*Xba*I cut fragment of *CESA7* promoter was ligated into *pGWB2* vector cut with *Hind*III (blunted) and *Xba*I to produce *pGWB2-proCESA7*. The coding sequence of *CESA7* was amplified with primers 5'-CCGGTACCATTGGAAGCTAGCGCCG-GT-3' and 5'-TCAGCAGTTGATGCCACACTTGGGAAGTGT-3'. The coding sequence of *GFP* was amplified with primers 5'-ATGGTGAGCAAGGGCGAGGAGCTGTTC-3' and 5'-CCG-GTACCCTTGTACAGCTCGTCCATGC-3'. Both *CESA7* and *GFP* were cut with *Kpn*I, ligated together to create the *GFP-CESA7* sequence, and PCR-amplified. *GFP-CESA7* was cloned into *pCR8/GW/TOPO* to produce *pCR8-GFP-CESA7* and confirmed by sequencing. To generate *proCESA7::GFP-CESA7*, a recombination reaction was performed between *pGWB2-proCESA7* and *pCR8-GFP-CESA7* using Gateway LR Clonase (catalog no. 12538-120; Invitrogen).

To generate the *35S::VND7-GR* construct, the coding sequence of *VND7* (*At1G71930*) was amplified with primers 5'-ATGGA-TAATAATGCAATCGTCAATGCCACC-3' and 5'-CCGGT-ACCCGAGTCAGGGAAGCATCCAAG-3' and the coding sequence of the receptor domain of the glucocorticoid receptor (*GR*) was amplified with primers 5'-CCGGTACCGGACCTCCTCCTG-GAGAAG-3' and 5'-TCATTTTGTATGAAACAGAAGCT-TTTTGATATTTTC-3'. Both *VND7* and *GR* were digested with *Kpn*I, ligated together to create *VND7-GR*, and PCR-amplified. *VND7-GR* was cloned into *pCR8/GW/TOPO* to produce *pCR8-VND7-GR* and confirmed with sequencing. *35S::VND7-GR* was created by using Gateway LR Clonase to perform a recombination reaction between *pGWB2(35S)* and *pCR8-VND7-GR*.

To produce the *proEB1b::mCherry-EB1b* construct, the promoter of *EB1b* (*At5G62500*) was amplified with primers 5'-CACCGG-TAAGAGTCTAGACTAGCTATGATCAATTT-3' and 5'-GCC-CTTGCTCACCATTGTTGAACCCCTCTCTGAAACGAA-3' (containing the overhang of a mCherry fragment); mCherry was amplified with primers 5'-GAGAGGGGTTCAAAAAT-GGTGAGCAAGGGCGAGGAGGATAA-3' (containing the overhang of the *EB1b* promoter fragment) and 5'-AATGTT-CGTCGCCATTGCTCCTGCTCCCTGTACAGCTCGTCC-ATGC-3' (containing overhangs of the "glycine-alanine" linker encoding sequence and the *EB1b* encoding fragment); *EB1b* genomic sequence was amplified with primers 5'-GAC-GAGCTGTACAAGGGAGCAGGAGCAATGGCGACGAA-CATTGGGATGA-3' and 5'-ATACCATTACTTTGTATTTCTT-TAAAGTGAAAATTC-3'. The above-mentioned three PCR fragments were further linked together by fusion PCR. The resulting PCR fragment was cloned into the *pENTR/D-TOPO* (catalog no. K2400-20; Invitrogen) vector to produce *pENTR-proEB1b::mCherry-EB1b*, confirmed with sequencing, and delivered into *pEarleyGate302* by recombination to get the final *proEB1b::mCherry-EB1b* construct.

**Spinning Disk Confocal Microscopy Imaging.** Seedlings were imaged between two glass coverslips. Transdifferentiating seedlings were prepared as described above, and slides were prepared with the induction medium described above. Imaging of CSC markers during PCW synthesis was conducted in epidermal cells 1–2 mm

below the apical hook of 3-d-old dark grown seedlings, a common model tissue for PCW synthesis. Seedlings used for imaging during PCW synthesis were grown on half-strength MS plates with 0% sucrose, and slides were prepared with half-strength MS liquid medium with 0% sucrose.

Images were acquired every 5 s for periods of 5–8.5 min to generate time-lapse movies to assess the localization, dynamics, and distribution of fluorescent protein-tagged proteins of interest. Photobleaching was caused by three rapid pulses with a 405-nm laser in designed ROIs. In lateral photobleaching experiments designed to visualize the directional movement of GFP-CESA particles (Fig. 2 C, F, I, and L and Movie S2), the two lateral regions of cells were bleached during time-lapse imaging. In these experiments, the bleach event occurred at the 2-min time point of 7-min time-lapse acquisition. In photobleaching experiments designed to measure the delivery rate of CSCs (Fig. 3B and Movie S3), a region that was ~20  $\mu$ m long and spanned the entire width of the cell was bleached at the 30-s time point of 8.5-min time-lapse acquisitions.

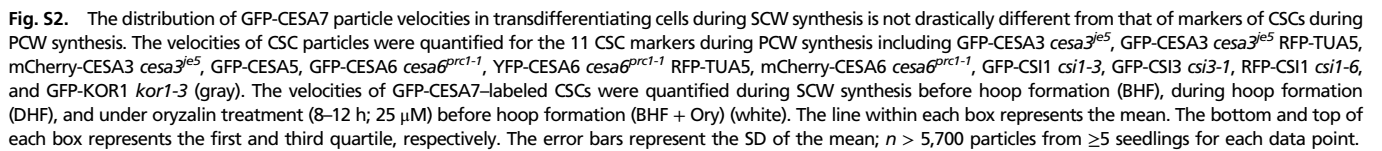
**Image Analysis.** The velocities of CSC particles were measured using the automated particle-tracking feature of Imaris software (Bitplane). Particle tracking parameters were set to exclude Golgi compartments and remove noise from the analysis. These parameters constrained the particle diameter to 250 nm and required each particle to be tracked continuously for more than 30 s (six frames). The accuracy of automated velocity measurements was confirmed by conducting manual kymograph-based particle velocity measurements in ImageJ (NIH).

The analysis of the direction of CSC particle movement along a track was performed through kymograph analysis on a track-by-track basis. Kymographs were generated using the multiple kymograph tool in ImageJ with a one-pixel line-width setting. Care was taken to select a single track for each kymograph and to minimize the possibility of capturing particles from multiple adjacent tracks within a single kymograph. For each kymograph, the number of particles that traveled from left-to-right and from right-to-left was recorded. The percentage of particles that moved in each direction was then calculated for each track. If a majority of particles moved in the same direction along a given track, that direction was assigned as the favored direction and the alternative direction was assigned as the opposed direction. If an equal number of particles moved in each direction along a track, "50%" was scored to both the "favored" and "opposed" direction dataset. A minimum of 48 kymographs and 6 seedlings from each experimental condition was used to calculate the average percentage of particles moving in the favored and opposed direction.

Lateral photobleaching experiments were conducted such that the two lateral sides of a cell were bleached, leaving a strip of unbleached GFP-CESA particles down the center of the cell. The movement of PM-localized GFP-CESA particles was then tracked for 5 min after photobleaching to discern whether the particles moved from the center strip to the left and/or right bleached region.

To analyze the correlation between directionally coherent GFP-CESA7 movement and CMT polarity, kymographs of both GFP-CESA7 and RFP-EB1b were generated from shared tracks. If 65% or more of EB1b particles were moving in a common direction, that direction was assigned as the microtubule plus-end of the track. If less than 65% of EB1b particles were moving in a common direction, the track was deemed not to have a well-defined microtubule polarity. Likewise, if 65% or more GFP-CESA7 particles were moving in a common direction, the track was considered to exhibit directionally coherent CSC movement either toward the





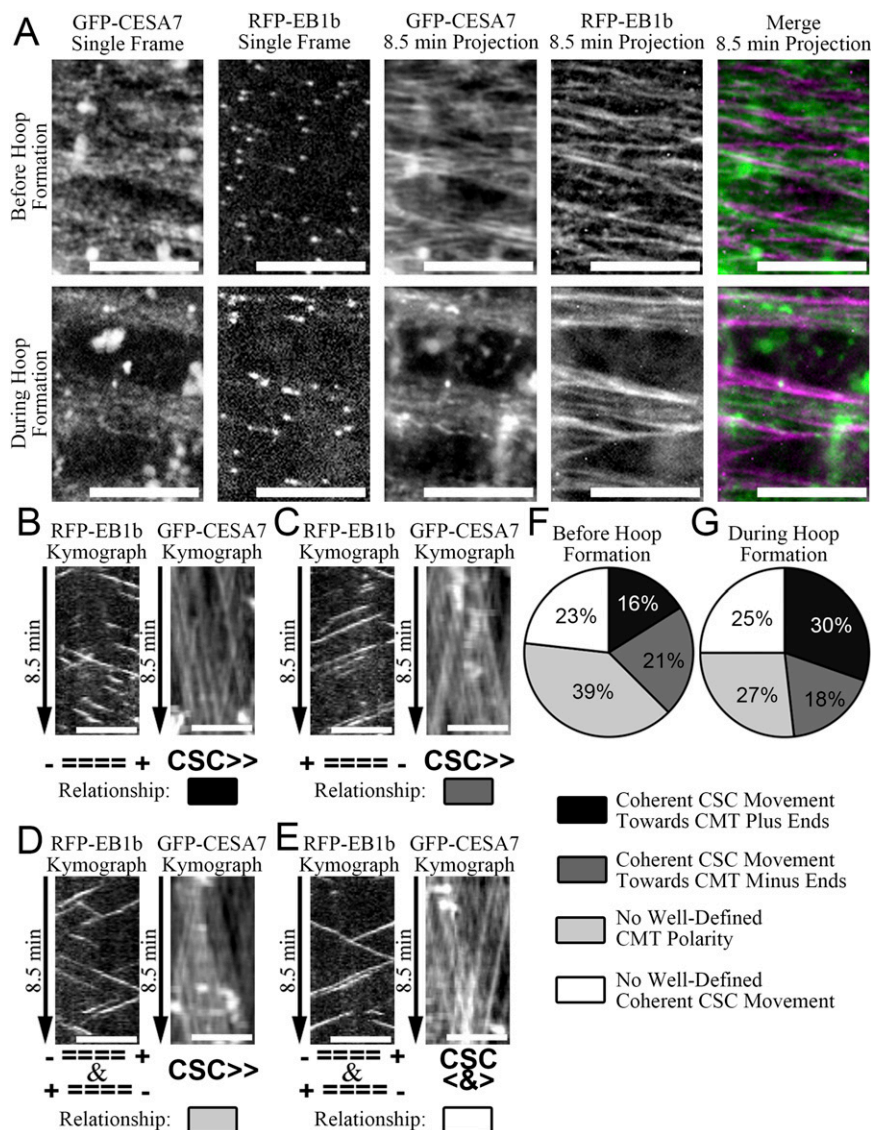
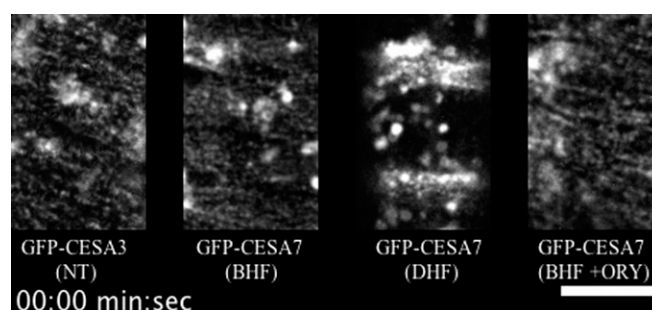


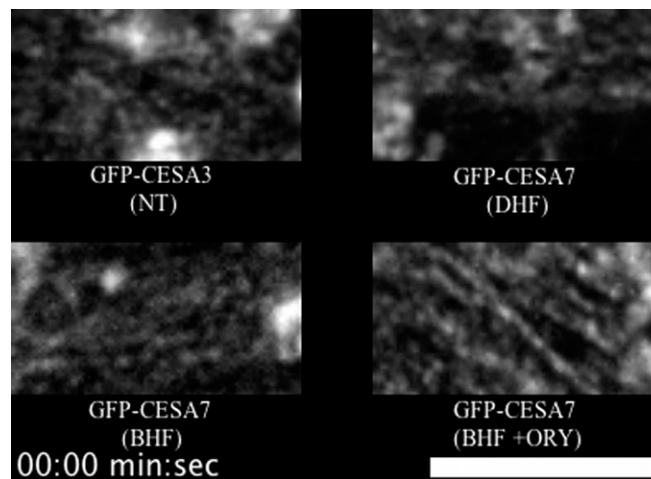
**Fig. S3.** The direction of coherent CSC movement is not correlated with the polarity of the CMTs along which the CSCs are moving. (A) In transdifferentiating cells, GFP-CESA7-labeled PM-localized CSCs traveled along trajectories that coincided with the trajectories of RFP-EB1b particles, which label the plus-ends of polymerizing microtubules, both before and during hoop formation. (Scale bars: 10  $\mu\text{m}$ .) (B–E) Kymograph analysis displays the direction of EB1b particle movement, from which the polarity of new microtubules can be deduced, and the direction of CSC particle movements from four representative tracks. (Scale bars: 5  $\mu\text{m}$ .) The direction of coherent CSC movement was occasionally toward the plus-ends of newly synthesized CMTs (B) or toward the minus-ends of newly synthesized CMTs (C). Some tracks did not exhibit a dominant CMT polarity (D and E) or coherent CSC movement (E). The relationship between the direction of coherent CSC movement and the polarity of newly synthesized CMTs was quantified before and during hoop formation (F and G). *N* is 56 tracks from 7 seedlings for each pie chart.

**Fig. S4.** Treatment with 25- $\mu$ M oryzalin for 8–12 h disrupts CMTs. (A) Motile RFP-EB1b particles demarcate newly polymerized CMTs in mock-treated seedlings. (B) RFP-EB1b no longer localizes to particles at the cell cortex in oryzalin-treated seedlings but rather displays a faint cytosolic signal, which suggests that CMT polymerization is abolished. (C and D) GFP-MAP4 localizes to CMTs in mock-treated seedlings (C) but is diffusely distributed throughout the cytosol in oryzalin-treated seedlings, which suggests that CMTs have depolymerized (D). (Scale bars: 10  $\mu$ m.)



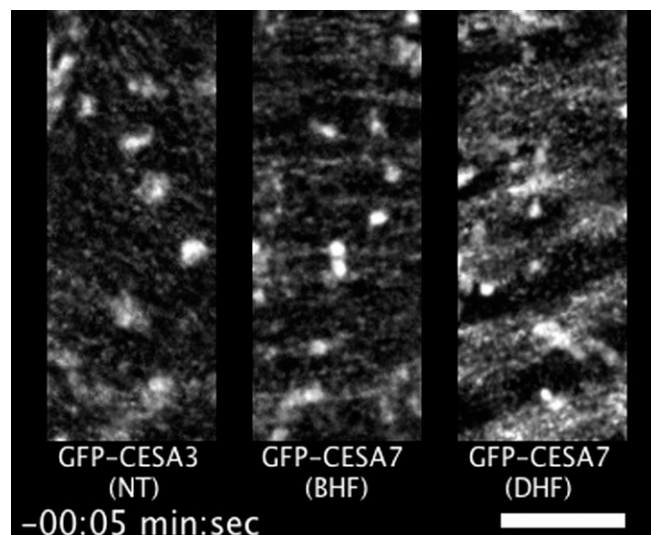
**Movie S1.** The dynamic characteristics of GFP-CESA3 during PCW synthesis and GFP-CESA7 during SCW synthesis at various stages of transdifferentiation are displayed by time-lapse imaging. CSC dynamics during PCW synthesis are represented by GFP-CESA3 particles in nontransdifferentiated (NT) seedlings. CSC dynamics during SCW synthesis is represented by GFP-CESA7 particles before hoop formation (BHF), during hoop formation (DHF), and under oryzalin treatment (BHF + ORY). The frame rate is 60 frames per second. (Scale bar: 10  $\mu\text{m}$ .)

Li et al. [www.pnas.org/cgi/content/short/1613273113](http://www.pnas.org/cgi/content/short/1613273113)



**Movie S2.** Lateral photobleaching experiments display the bidirectional movement of GFP-CESA3 particles during PCW synthesis and the directionally coherent movement of GFP-CESA7 particles during SCW synthesis. Time-lapse imaging was conducted for 2 min before photobleaching the lateral edges of the cells. In PCW-synthesizing nontransdifferentiated (NT) seedlings, GFP-CESA3 particles on a shared track move equally into the right and left bleached areas during PCW synthesis. In contrast, GFP-CESA7 particles on a shared track move either into the left or right bleached area during SCW synthesis both before (BHF) and during (DHF) hoop formation. Oryzalin treatment (BHF + ORY) did not disrupt the directionally coherent movement of GFP-CESA7 particles during SCW synthesis. The frame rate is 15 frames per second. (Scale bar: 10  $\mu$ m.)

[Movie S2](#)



**Movie S3.** The delivery of new CSCs to the PM is visualized after photobleaching during PCW synthesis and during SCW synthesis. The movie displays a single frame before photobleaching, followed by a single frame immediately after photobleaching and a 5-min period after photobleaching during which GFP-CESA particles repopulated the bleached region through the delivery of new CSCs to the PM. GFP-CESA3 particles in nontransdifferentiated (NT) seedlings represent CESA delivery during PCW synthesis, and GFP-CESA7 particles before hoop formation (BHF) and during hoop formation (DHF) represent CSC delivery during SCW synthesis. The frame rate is 15 per second. (Scale bar: 10  $\mu$ m.)

[Movie S3](#)